iScience

Article

Microglia target synaptic sites early during excitatory circuit disassembly in neurodegeneration

Graphical abstract

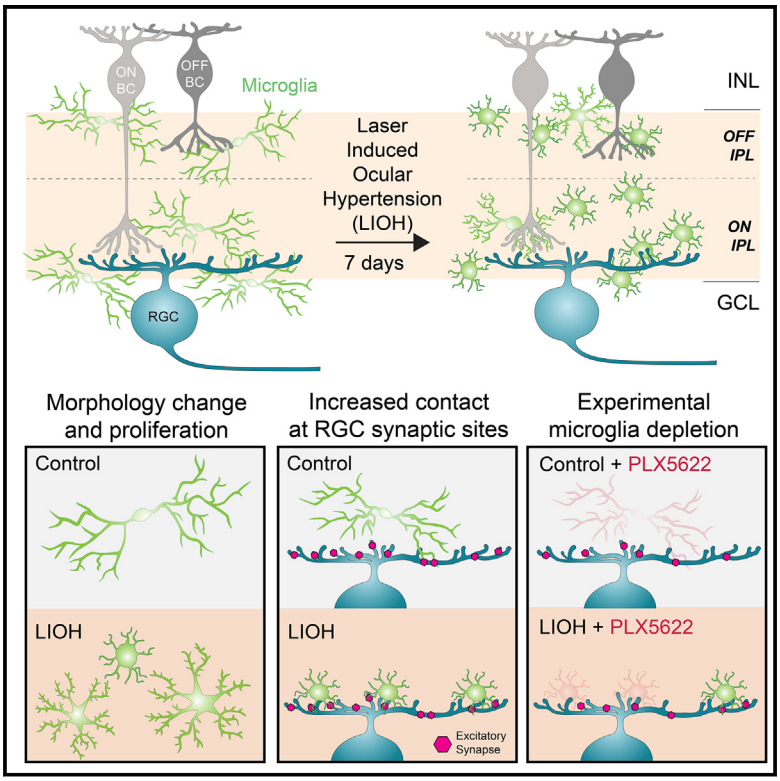

Highlights

- Early after IOP elevation, microglia increase in number, complexity, and process movement
- Microgliosis results in greater microglia-synaptic contact in the inner plexiform layer
- Microgliosis leads to greater contact with synapses on ganglion cell dendrites
- Microglia depletion results in improved ganglion cell function

Authors

Alfred Yu, Camille Fang, Li Xuan Tan, Aparna Lakkaraju, Luca Della Santina, Yvonne Ou

Correspondence

yvonne.ou@ucsf.edu

In brief

Natural sciences; Biological sciences; Neuroscience; Cellular neuroscience

Yu et al., 2025, iScience *28*, 112201
April 18, 2025
https://doi.org/10.1016/j.isci.2025.112201

CellPress

iScience

CellPress
OPEN ACCESS

Article

Microglia target synaptic sites early during excitatory circuit disassembly in neurodegeneration

Alfred Yu,[1] Camille Fang,[1] Li Xuan Tan,[1,2] Aparna Lakkaraju,[1] Luca Della Santina,[1,3] and Yvonne Ou[1,4,*]
[1]Department of Ophthalmology, UCSF School of Medicine, San Francisco, CA, USA
[2]School of Health and Life Sciences, University of Health and Rehabilitation Sciences, Qingdao, Shandong, China
[3]College of Optometry, University of Houston, Houston, TX, USA
[4]Lead contact
*Correspondence: yvonne.ou@ucsf.edu
https://doi.org/10.1016/j.isci.2025.112201

SUMMARY

During development, microglia prune excess synapses to refine neuronal circuits. In neurodegeneration, understanding the role of microglia-mediated synaptic pruning in circuit remodeling and dysfunction is important for developing therapies aimed at modulating microglial function. Here, we analyzed microglia-mediated synapse disassembly of degenerating postsynaptic neurons in the inner retina. After inducing transient intraocular pressure elevation to injure retinal ganglion cells, microglia increase in number, shift to hyper-ramified morphology, and exhibit greater process movement. Furthermore, due to the greater number of microglia, there is increased colocalization of microglia with synaptic components throughout the inner plexiform layer and with excitatory synaptic sites along individual ganglion cell dendrites. Microglia depletion partially protects ganglion cell function, suggesting that microglia activation may be neurotoxic in early neurodegeneration. Our results demonstrate the important role of microglia in synapse disassembly in degenerating circuits, highlighting that microgliosis is the primary mechanism for increased synapse colocalization early after neuronal injury.

INTRODUCTION

High-fidelity circuit function and homeostasis are dependent on appropriate and productive interactions among diverse cell types. Microglia are the highly dynamic resident immune cells of the central nervous system (CNS) that play diverse roles in surveilling the microenvironment and respond rapidly to tissue infection and injury. In addition to their role in immunity, microglia play a role in synapse remodeling and homeostasis, especially during development, when the emergence of functional neural circuits requires the formation and elimination of synapses, a process known as synaptic pruning or elimination. Microglia-mediated synaptic pruning is critical in removing weak or supernumerary synapses during circuit refinement.[1] For example, during visual circuit development, supernumerary nascent synapses are tagged with complement molecules C1q and C3, allowing microglia to recognize these excess synapses for phagocytosis.[2,3] Indeed, during development, microglia regulate laminar organization of neurons, promote cell death, limit axon outgrowth, and guide vascular networks,[4] making them crucial to circuit formation. In the disease context it has been suggested that aberrant reactivation of developmental programs of synapse pruning may result in neural circuit dysfunction.[5] Under pathological insult, microglia rapidly change their morphology and expression of signaling molecules to respond to injury. This dysregulated microglial activity can eliminate both healthy and dysfunctional synapses, impairing synaptic connectivity and ultimately circuit function.[1,6]

Synapse disassembly is an early hallmark of neurodegeneration, including during the progressive loss of ganglion cells in glaucoma, a blinding disease for which the role of retinal microglia and neuroinflammation is becoming better understood both in animal models and in human postmortem tissue.[7–13] In the retina, microglia occupy distinct regions that include the synaptic layers, the outer plexiform layer (OPL) and the inner plexiform layer (IPL). Notably, mounting evidence highlights retinal and optic nerve microglia activation as an early event in rodent models of experimental glaucoma,[14–17] although whether microglia serve a neuroprotective or neurotoxic role remains a controversial question.[18–24] Furthermore, the activation of microglia in the retinal IPL, their interaction with synapses, and their role in synapse disassembly in experimental glaucoma remain unclear.

Previously, we demonstrated that an early event in glaucomatous neurodegeneration is a reduction of synapse density on individual alpha ganglion cells prior to dendrite retraction and cell death.[9] More recently, we showed that after transient elevation of intraocular pressure (IOP), synapse loss occurs throughout the retinal IPL in a sublamina-dependent fashion.[25] Here, after transient IOP elevation, activated microglia increase in density throughout the IPL, increase their motility, and exhibit

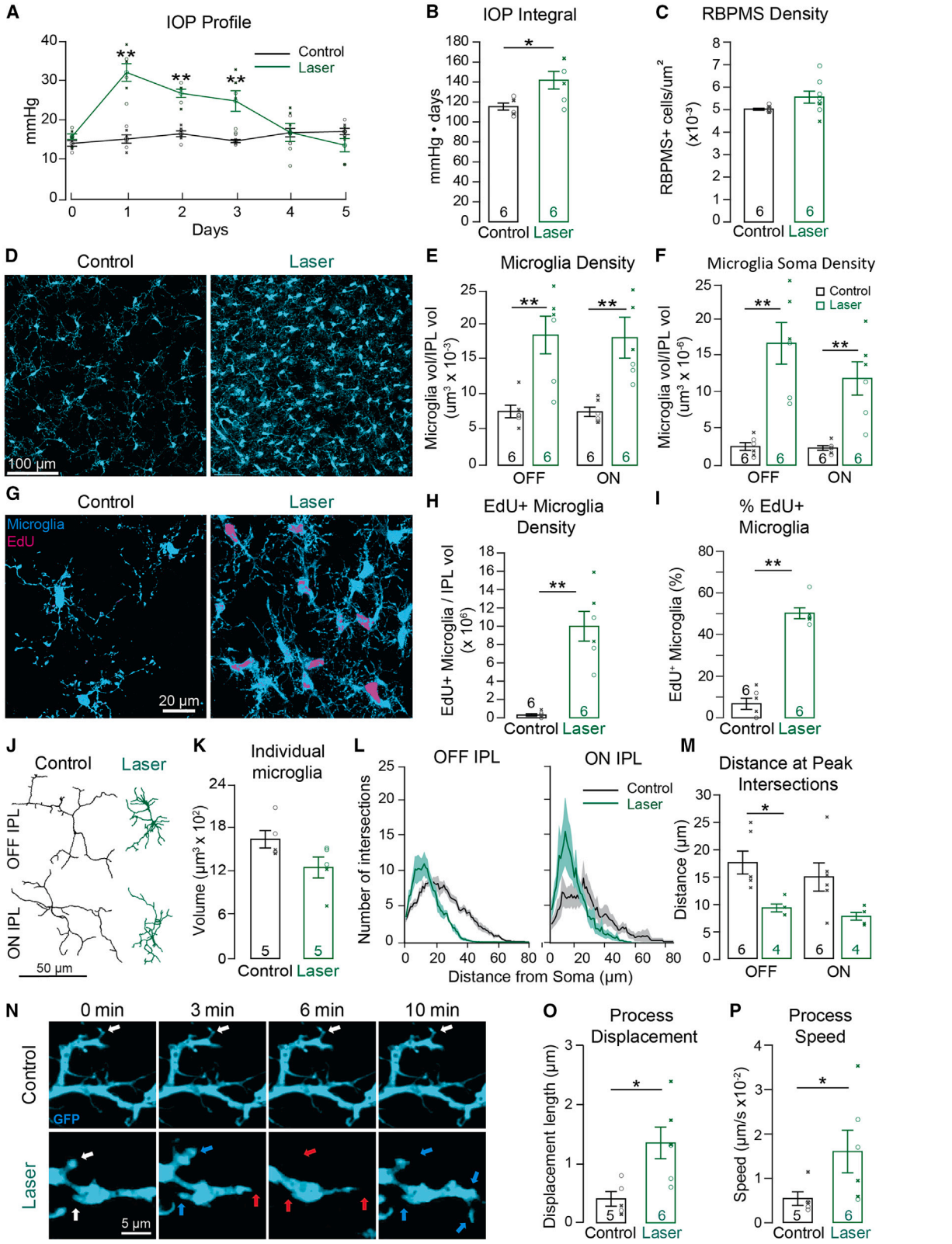

(legend on next page)

colocalization with synaptic components. Due to their increased density, microglia increase contact with individual ganglion cell synaptic sites, including both intact synapses and disassembled synapses where the presynaptic component was absent. However, microglia depletion did not result in excitatory synapse preservation but partially protected against loss of ganglion cell function. Taken together, these experiments suggest that microglia play a role in the disassembly of synaptic connections by increasing in number after neuronal injury and colocalizing with synaptic components at excitatory synaptic sites on degenerating ganglion cell dendrites.

RESULTS

After IOP elevation, microglia increase in number, complexity, and motility in the IPL

In order to assess the role of microglia in synapse disassembly of degenerating postsynaptic neurons, we used a laser-induced ocular hypertension (LIOH) model to transiently elevate IOP in $CX_3CR\text{-}1^{GFP}$ mice, which results in retinal ganglion cell (RGC) loss but not until 14 days after IOP elevation.[9,11,25,26] Peak IOP occurs 24 h after the laser procedure, returning to baseline 5 days after treatment (Figure 1A). The IOP integral is higher in the lasered eyes (141.8 ± 8.8 mmHg · days) vs. control eyes (115.4 ± 3.5 mmHg · days) ($p = 0.03$), but there is no difference in RGC density as identified via immunolabeling using an antibody to RNA-binding protein with multiple splicing (RBPMS) at this 7 days time point (Figures 1B and 1C). In all experiments we examined the 7 days-post LIOH time point at which IOP has returned to baseline levels and is the earliest time point that we observe synapse loss on individual ganglion cells but no significant RGC death.[9]

Microglia are activated in the IPL following IOP elevation as demonstrated by recruitment and proliferation of microglia, a shift in morphology, and increased motility of microglia processes. The IPL was divided into volumetric percentile bins, where 0–40% from the INL/IPL border represents the OFF sublamina and 40–100% (100% at the IPL/GCL border) represents the ON sublamina (Figure S1).[27] After IOP elevation, microglia volume and number are significantly elevated in the IPL in both the ON and OFF sublaminae (Figures 1D–1F, OFF sublamina LIOH 0.018 ± 0.003 vs. CTL 0.008 ± 0.001 cells/μm^3, $p = 0.008$, ON sublamina LIOH 0.019 ± 0.003 vs. CTL 0.008 ± 0.001 cells/μm^3, $p = 0.005$). To determine whether the increase in microglia population in the IPL is due to proliferation rather than recruitment or infiltration from the ganglion cell layer (GCL) or outer plexiform layer (OPL), an EdU (5-ethynyl-2′-deoxyuridine) cell proliferation assay was performed and ∼50% of activated microglia is the result of proliferation during the period of IOP elevation (Figures 1G–1I, LIOH 20.92 ± 7.20 vs. CTL 0.63 ± 0.68 cells/μm^3, $p = 0.005$). When EdU^+ vs. EDU^- microglia was compared, there were no significant differences in morphological parameters such as microglia size and complexity (Figures S1D–S1J). The change in morphology of individual microglia in the control vs. laser conditions can be appreciated in the representative skeletons (Figure 1J), in which activated microglia are decreased in volume (Figure 1K). Sholl analysis of individual microglia quantified the complexity of branching of microglia processes. Following IOP elevation, microglia exhibited an increase in the number of intersections as well as a decrease in the distance that the peak intersections occurred, consistent with a more hyper-ramified morphology in both the ON and OFF sublaminae (Figures 1L and 1M). To assess microglia dynamics 7days after IOP elevation, retinas were explanted and cultured, and microglia in the ON sublamina were imaged live using spinning disk confocal microscopy. We observed rapid movement of activated microglia processes (Figures 1N–1P), with microglia process displacement (LIOH 1.35 ± 0.11 vs. CTL 0.40 ± 0.06 μm, $p = 0.02$) and process speed significantly increased following IOP elevation (LIOH 0.016 ± 0.002 vs. CTL 0.005 ± 0.001 μm/s, $p = 0.03$).

Microglia-synaptic contacts increase in the IPL after transient IOP elevation

To determine whether microglia play a role in synapse disassembly or engulfment, we examined synaptic protein colocalization within individual microglia by immunolabeling with an excitatory postsynaptic density scaffolding protein (PSD95) and a presynaptic ribbon protein (CtBP2) (Figure 2A). We used ObjectFinder to identify all excitatory synapses colocalized inside microglia across volumes of IPL (Figure S1).[25,28] The

Figure 1. After IOP elevation, microglia increase in number, complexity, and process movement in the IPL

(A) IOP was measured daily following laser-induced ocular hypertension (LIOH), with IOP returning to baseline by day 5.

(B) The lasered eye exhibited a higher IOP integral compared to the contralateral control eye.

(C) Quantification of $RBPMS^+$ cells shows no ganglion cell loss 7 days after IOP elevation.

(D) Representative maximum intensity projections of microglia (cyan) in the IPL of control and laser conditions.

(E and F) Volumetric density of microglia within the IPL is calculated in both the ON and OFF sublaminae (E) as well as (F) density of microglia soma.

(G) Representative images of EdU labeling (magenta) of microglia (cyan) in control and laser conditions are quantified as (H) EdU^+ microglia density in the IPL and (I) percentage of microglia in the IPL that are EdU^+. (C-I) Individual values were obtained from an average of 4 z stack images taken at the central regions of the retina in 4 leaflets.

(J) Representative skeletons of individual microglia.

(K–M) Quantification of (K) individual microglia volume, (L) Sholl analysis of microglial processes, solid lines represent mean values, shaded areas represent ±SEM for control in black and laser in green. (M) Distance at peak intersection to determine complexity of microglia processes. (J–M) Microglia morphology was assessed in the central region of the 4 leaflets considering only fully intact microglia in the entire image stack.

(N) Live imaging of microglia in *ex vivo* explant preparation acquired for 5 to 10 min; representative stills are presented here at 0, 3, 6, and 10 min. White arrows indicate baseline location and no change in movement. Cyan arrows indicate areas of extension and red arrows indicate areas of retraction.

(O and P) Movement of microglia processes was quantified as (O) total process displacement and (P) process speed using the surface tool in Imaris. 2–6 microglia were analyzed from 5 control and 6 lasered animals. Bars represent mean ± SEM with black and green bars representing control and laser condition respectively. The number of animals (n) is reported in each histogram, with individual values of each male animal represented by "x" and female by "o" markers, respectively. Statistics: Mann-Whitney U test; * <0.05, ** <0.01.

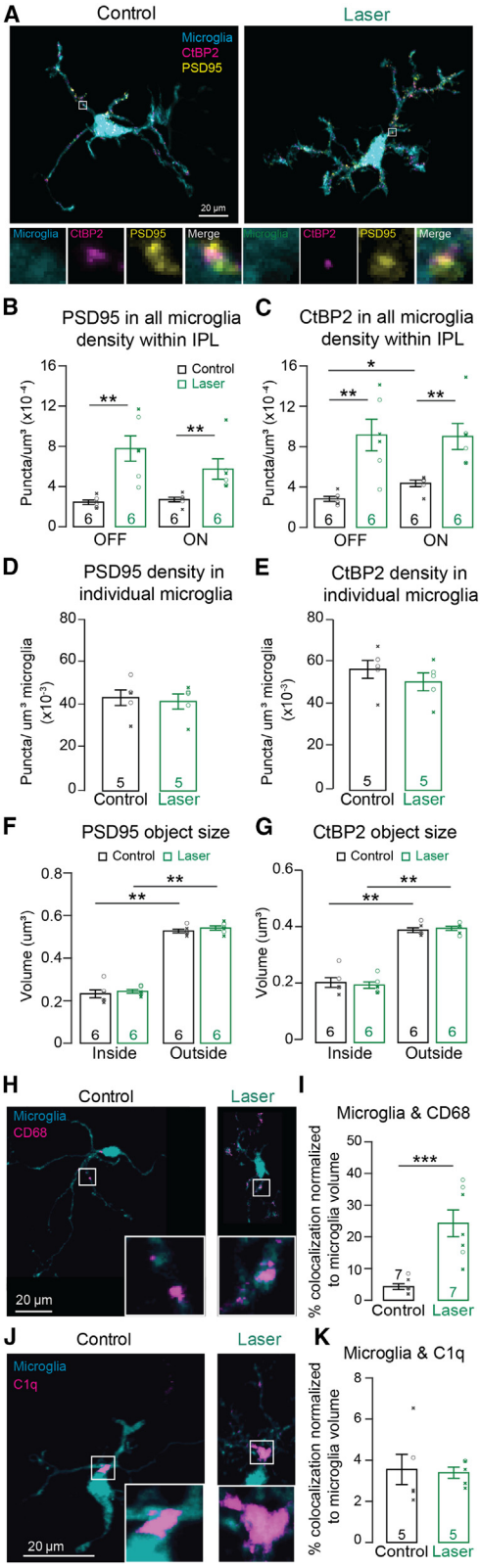

Figure 2. Microglia-synaptic contacts increase in the IPL after transient IOP elevation

(A) Confocal image stacks of an individual microglia (cyan) with engulfed PSD95 (yellow) and CtBP2 (magenta) puncta in control and laser conditions. Below are zoomed in areas of the white bounding box with each signal separated and merged.

(B and C) PSD95 puncta density (B) and CtBP2 density (C) in total microglia volume in the OFF and ON sublamina of the IPL.

(D and E) PSD95 density (D) and CtBP2 density (E) in individual microglia volume.

(F and G) PSD95 (F) and CtBP2 (G) puncta volume was analyzed inside and outside of microglia.

(H) Representative images of microglia (cyan) and CD68 (magenta) in control and laser condition.

(I) Colocalized volume between microglia and CD68.

(J) Representative images of microglia (cyan) and C1q (magenta) in control and laser condition.

(K) Colocalized volume between microglia and C1q. Zoomed in insets of the white bounding box is presented in the lower right corner of each image. Bars represent mean ± SEM with black and green bars representing control and laser, respectively. The number of animals (n) is reported in each histogram, with individual values of each male animal represented by "x" and female by "o" markers, respectively. Z-stacks were acquired from the central region of 4 leaflets of each retina and averaged. Statistics: Mann-Whitney U test; * <0.05, ** <0.01, *** <0.001.

population of microglia in the IPL increased engulfment of PSD95 and CtBP2 puncta, as quantified by the density of PSD95 and CtBP2 within microglia volume in the IPL (Figures 2B and 2C). Dividing the IPL into the ON and OFF sublamina revealed that the increase in PSD95 and CtBP2 engulfment is occurring in both the OFF and ON sublamina of the IPL (PSD95: OFF LIOH 7.78 ± 1.26 $*10^{-4}$ vs. CTL 2.44 ± 0.22 $*10^{-4}$ puncta/μm^3, p = 0.005; ON LIOH 5.73 ± 0.10$*10^{-4}$ vs. CTL 2.71 ± 0.23$*10^{-4}$ puncta/μm^3, p = 0.005; CtBP2: OFF LIOH 9.15 ± 1.56 $*10^{-4}$ vs. CTL 2.82 ± 0.024 $*10^{-4}$ puncta/μm^3, p = 0.008; ON LIOH 9.00 ± 1.28$*10^{-4}$ vs. CTL 4.35 ± 0.32$*10^{-4}$ puncta/μm^3, p = 0.005). When analyzing PSD95 and CtBP2 puncta density colocalized within each individual microglia (Figures 2D and 2E), there was no significant difference between conditions (PSD95: LIOH 0.042 ± 0.004$*10^{-3}$ vs. CTL 0.044 ± 0.004$*10^{-3}$ puncta/μm^3, p = 0.75; CtBP2: LIOH 0.051 ± 0.004$*10^{-3}$ vs. CTL 0.057 ± 0.005$*10^{-3}$ puncta/μm^3, p = 0.18). It has been shown in hippocampus organotypic tissue culture that rather than whole synapse engulfment, microglia prune presynaptic components via trogocytosis, or "nibbling," engulfing small (<1 micron) presynaptic components.[29] Therefore, we next examined the size of synaptic puncta colocalized inside microglia. Analysis of PSD95 puncta size showed that PSD95 engulfed within microglia have a significantly smaller average volume compared to PSD95 puncta that do not colocalize within microglia, which was true for both control and laser conditions (Figure 2F, LIOH engulfed 0.24 ± 0.01 vs. non-engulfed 0.54 ± 0.01 μm^3 p = 0.005, CTL engulfed 0.23 ± 0.02 vs. non-engulfed 0.52 ± 0.01 μm^3, p = 0.005). This difference was also observed for CtBP2 inside compared to CtBP2 outside of microglia (Figure 2G, LIOH engulfed 0.27 ± 0.02 vs. non-engulfed 0.54 ± 0.01 μm^3, p = 0.005; CTL engulfed 0.28 ± 0.03 vs. non-engulfed 0.53±-0.01 μm^3, p = 0.005).

We next wanted to examine the functional phenotype of these activated microglia by assessing known markers of

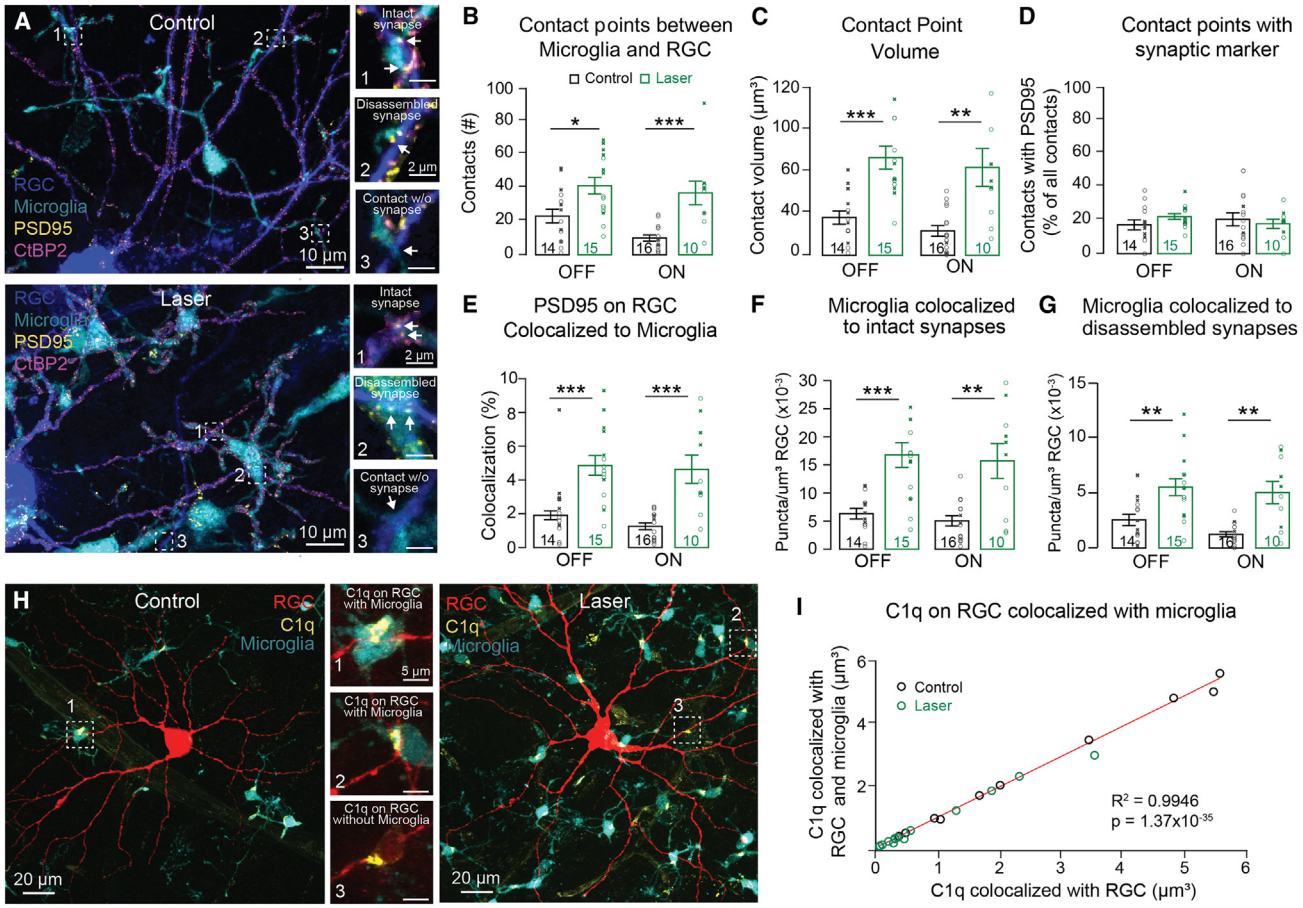

Figure 3. Microglia target synapses on alpha RGCs following IOP elevation

(A) Representative image of labeling of a single retinal ganglion cell (blue) with microglia (cyan), PSD95 (yellow), and CtBP2 (magenta), see also Figure S1. Zoomed-in area with an intact synapse (PSD95 and CtBP2 puncta in apposition), an area with a disassembled synapse (PSD95 with no CtBP2 puncta), and an area of microglia contact with RGC without CtBP2 and PSD95.

(B–D) Quantification of the contact between microglia and individual cell dendrites is presented as (B) number of individual contacts, (C) the total volume of contact and (D) the percentage of contact points colocalized with PSD95.

(E–G) Colocalization analysis was performed to determine (E) the percentage of PSD95 on the ganglion cell colocalized with microglia; (F) the density of microglia colocalized with intact synapses on an individual ganglion cell; and (G) the density of microglia colocalized with disassembled synapses on an individual ganglion cell.

(H) Representative images of labeling of a single RGC with C1q and microglia with zoomed in insets examples of area C1q colocalization to RGC/microglia contact points in control and laser conditions (1–2), and areas of C1q colocalization on RGC without microglia (3).

(I) Correlation plot between C1q volume colocalized on RGC dendrites (abscissa) and C1q volume colocalized with RGC dendrites and microglia (ordinata). After performing linear regression analysis with 95% confidence level, R^2 and p value are reported in the chart. Bars represent mean ± SEM with black and green bars representing control and laser conditions respectively. The number of cells (n) is reported in each bar from 6 mice for OFF cells and 3 mice for ON cells (1–6 cells per retina). In all plots, individual values from male animals are represented by "x" and female by "o" markers, respectively. Statistics: Mann-Whitney U test; * <0.05, ** <0.01, *** <0.001.

microglia activation and phagocytosis. CD68, a marker of microglia activation, is upregulated in microglia following IOP elevation. The colocalized volume between microglia and CD68 (normalized to microglia volume) throughout the IPL is significantly increased (Figures 2H and 2I, LIOH 24.9 ± 4.2% vs. CTL 4.3 ± 0.9%, p = 0.0006). C1q, a protein complex involved in the complement pathway and known signaler of microglia for phagocytosis, is unchanged when normalized to microglia volume following IOP elevation (Figures 2J and 2K, LIOH: 3.4 ± 0.3% vs. CTL 3.6 ± 0.8%, p = 0.69). Therefore, although the density of synaptic components within individual microglia was unchanged in control and LIOH conditions, activated microglia exhibited increased expression of phagocytic marker CD68.

Microglia target synapses on alpha ganglion cells following IOP elevation

Using the $CX_3CR\text{-}1^{GFP}$ mouse along with ballistic labeling of individual RGCs and immunolabeling of synaptic components, we evaluated microglial activation and their role in synapse disassembly at the individual RGC level (Figure S1). To determine microglial interaction with RGCs, individual ganglion cells

were ballistically labeled with dextran dye and microglia interaction with synaptic proteins within the ganglion cell was analyzed (Figure 3A). Alpha ganglion cells (αRGCs) were identified based on their large soma size and characteristic dendritic architecture.[30] To identify the number of contact points between microglia and individual αRGCs, we colocalized their respective signals and measured the overlapping volume, observing that both number (OFF: LIOH 41.5 ± 4.9 vs. CTL 23.2 ± 4.1, p = 0.03; ON: LIOH 37.1 ± 7.0 vs. CTL 10.1 ± 1.8 contacts, p = 0.0003) and volume (OFF: LIOH 69.4 ± 8.2 vs. CTL 26.8 ± 4.7 μm^3, p = 0.0002; ON: LIOH 62.4 ± 13.5 vs. CTL 17.3 ± 3.8 μm^3, p = 0.001) of contact points is increased in the laser condition (Figures 3B and 3C). However, when we examined only the fraction of RGC dendrite-microglia contact points that included PSD95, there was no significant difference in the control vs. laser condition (Figure 3D OFF: LIOH 22.4 ± 1.7% vs. CTL 17.4 ± 3% p = 0.13, ON: LIOH 18.0 ± 3% vs. CTL 20.7 ± 4%, p = 0.85). We further observed that these RGC dendrite-microglia contact points with PSD95 are specific, since rotation of the microglia channel by 90° in the xy-plane and 180° in the z-plane resulted in significantly decreased colocalization (Figure S2B). Next, we examined all PSD95 sites within each individual RGC and observed that the percentage of PSD95 puncta colocalized with microglia in the laser condition significantly increased in both OFF- and ON-stratifying αRGCs (Figure 3E; OFF: LIOH 4.8 ± 0.6 vs. CTL 1.9 ± 0.3%, p = 0.0004; ON: LIOH 4.6 ± 0.8 vs. CTL 1.3 ± 0.2%, p = 0.0005). Because it has been shown that microglia prune or ''trogocytose'' presynaptic components in hippocampus,[29] we examined microglia colocalization with intact synapses (defined as colocalization with both pre- and postsynaptic components on the ganglion cell dendrite) and disassembled synapses (defined as colocalization with PSD95 only on the ganglion cell dendrite missing a presynaptic ribbon). When we analyzed colocalization of microglia with intact (Figure 3F) and disassembled synapses (Figure 3G), we observed a significant increase in colocalization with both intact and disassembled synapses in both OFF- and ON-stratifying αRGCs following IOP elevation (Intact synapses OFF: LIOH 16.8 ± 2.2 vs. CTL 6.3 ± 0.9 puncta/μm3 ($x10^{-3}$), p = 0.0008; ON: LIOH 15.7 ± 3.1 vs. CTL 5.1 ± 0.9 puncta/μm3 ($x10^{-3}$), p = 0.005. Disassembled synapses OFF: LIOH 5.5 ± 0.8 vs. CTL 2.5 ± 0.5 puncta/μm3 ($x10^{-3}$), p = 0.004; ON: LIOH 5.0 ± 1.0 vs. CTL 1.3 ± 0.2 puncta/μm3 ($x10^{-3}$), p = 0.003). During visual system development, C1q tags synapses destined for elimination,[2] thus we examined whether C1q was colocalized with both the RGC dendrite and microglia (Figure 3H). When C1q was observed colocalized with an RGC dendrite, microglia were also often present at this site, with a relationship linearly proportional to the number of C1q puncta colocalized on the RGC's dendrite in both control and laser conditions (Figure 3I). This data demonstrate that microglia are targeting C1q-tagged synaptic sites rather than simply making random contacts with the ganglion cell dendrites. Taken together, these results demonstrate that microglia are targeting both synaptic sites (PSD95) and contact points where C1q is present, and that the increased colocalization with synaptic sites on individual RGCs is due to microgliosis.

Microglia depletion partially restores RGC function following IOP elevation

To assess whether microglia play a neurotoxic or neuroprotective role on RGC structure and function after IOP elevation, we depleted microglia by administering PLX5622, a CSF1R inhibitor (Figure 4A). When PLX5622 was administered via diet we observed ∼96% depletion of microglia in the IPL in control eyes (CTL 209.9 ± 39.0 vs. CTL+PLX 9.2 ± 10.4 microglia/μm^2, p = 0.02). Lasered eyes from the same animals that were on PLX5622 diet had a significant increase in microglia density compared to control eyes from animals on PLX5622 (CTL+PLX 9.2 ± 10.4 vs. LIOH+PLX 208.3 ± 166.5 microglia/μm^2, p = 0.039), however, it was decreased when compared to control eyes from animals on normal chow and significantly decreased when compared to lasered eyes from animals on normal chow (Figure 4B, LIOH 858.6 ± 598.2 vs. LIOH+PLX 208.3 ± 166.5 microglia/μm^2, p = 0.01). We next examined PSD95 puncta colocalized with individual ON and OFF alpha ganglion cell dendrites (Figure 4C) and observed a significant decrease in PSD95 density in control eyes from animals on PLX5622 chow compared to control eyes from animals on normal chow (OFF PLX 0.339 ± 0.018 vs. non-PLX 0.465 ± 0.017 puncta/μm^3, p = 0.003; ON PLX 0.302 ± 0.031 vs. non-PLX 0.506 ± 0.018 puncta/μm^3, p = 0.000002). Furthermore, laser and control eyes from animals on PLX5622 diet showed comparable reductions in PSD95 density on ON and OFF αRGCs compared to laser and control eyes from animals on normal chow (Laser OFF: PLX 0.366 ± 0.031 vs. non-PLX 0.453 ± 0.019 puncta/μm^3, p = 0.03; Laser ON: PLX 0.304 ± 0.033 vs. non-PLX 0.418 ± 0.017 puncta/μm^3, p = 0.014). We next examined RGC function by performing pattern electroretinograms (PERGs), in which a black-white horizontal grating is presented with a square wave profile. The PERG waveform reflects inner retina activity, with a positive wave peaking at ∼80 ms (P1) and a broad wave peaking at ∼300 ms (N2).[31] Following IOP elevation, both the P1 and N2 amplitudes of the PERG were significantly decreased (Figures 4D–4F; P1 LIOH 2.92 ± 0.47 vs. CTL 8.44 ± 0.50 μV, p = 0.025; N2 LIOH -4.51 ± 0.61 vs. CTL -12.14 ± 0.73 μV, p = 0.0007). With microglia depleted prior to and for 7 days during and after IOP elevation there was a significant increase in P1 and N2 amplitude compared to lasered animals on normal chow (P1 LIOH+PLX 5.67 ± 0.43 vs. LIOH 2.92 ± 0.47 μV, p = 0.02; N2 LIOH+PLX -7.66 ± 0.71 vs. LIOH -4.51 ± 0.61 μV, p = 0.03). Taken together, these data suggests that microglia may play a role in maintaining synapses in the control condition but are neurotoxic when in an activated state.

DISCUSSION

The role of microglia in synapse disassembly in neurodegeneration of mature circuits is not well understood. Here, we show that microglia activation occurs throughout the IPL early after IOP elevation, at a time point well before ganglion cell death. Microglia increase in number, complexity, and process movement after transient IOP elevation. Due to microgliosis, activated microglia as a population in the IPL increase their colocalization with synaptic components, increase their contact with individual ganglion cells, and target synaptic sites on both ON and OFF

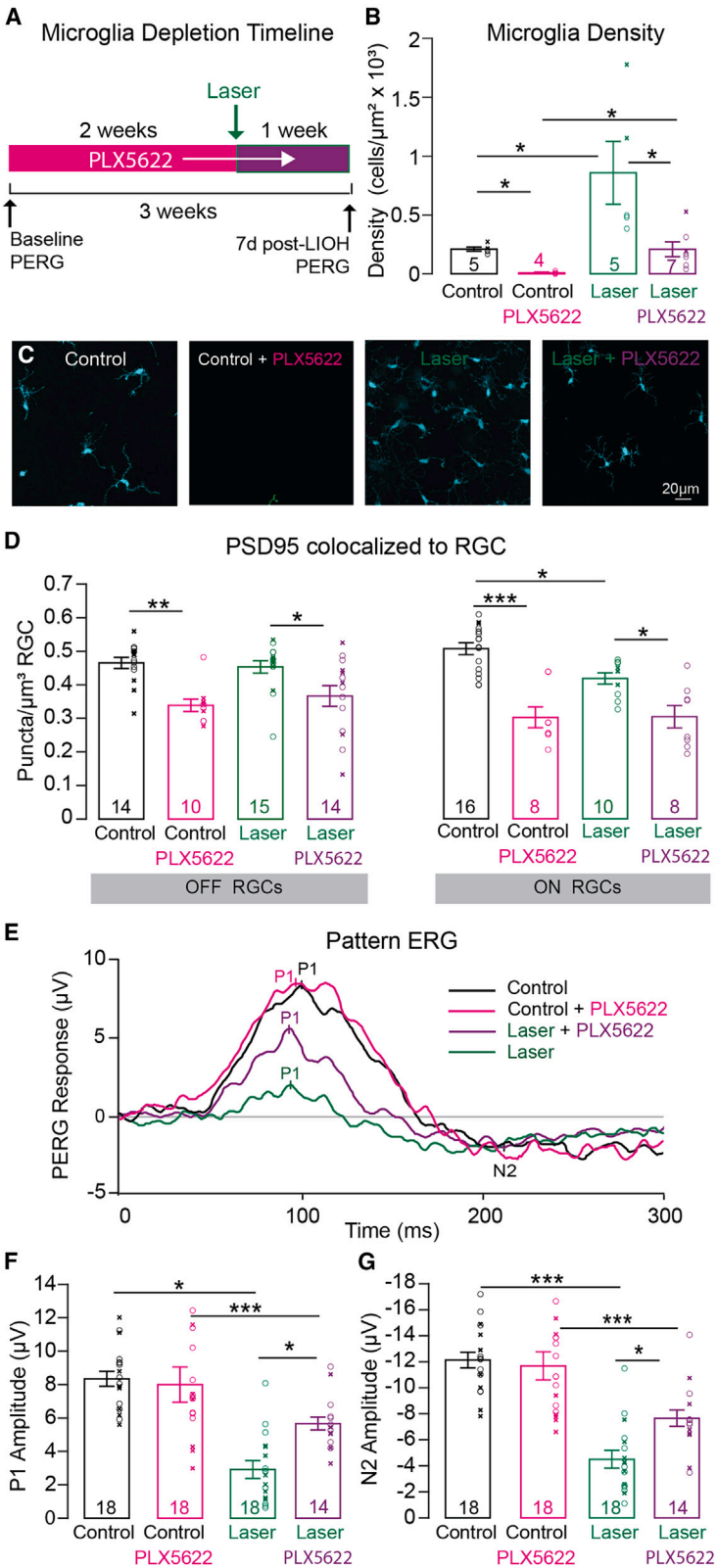

Figure 4. Microglia depletion partially restores RGC function following IOP elevation

(A) Experimental design and timeline of PLX5622 treatment, PERG recording, and laser-induced ocular hypertension. Following PLX5622-induced microglia depletion.

(B) The volume of microglia was measured in control (black bar), control with PLX5622 treatment (magenta), laser condition (green), and laser condition animals on PLX5622 treatment (purple). The number of animals (n) is reported in each histogram.

(C) Representative maximum intensity projection images of IPL microglia in control and laser conditions with and without PLX5622 treatment.

(D) Colocalization analysis of PSD95 on individual ON and OFF alpha ganglion cells is represented as synapse density across the four experimental groups. The number of cells (n) is reported in each histogram from 4 to 7 animals.

(E) Representative PERG traces of the four experimental groups.

(F and G) Analysis of PERG amplitude (F) P1 and (G) N2 was quantified. Bars represent mean ± SEM. The number of animals (n) is reported in each histogram. In all plots, individual values from male animals are represented by "x" and female by "o" markers, respectively. Statistics: Mann-Whitney U test; * <0.05, ** <0.01, *** <0.001, **** <0.0001.

alpha ganglion cell dendrites. Activated microglia increase expression of phagocytic protein CD68, but remarkably individual microglia do not exhibit an increased density of colocalized synaptic puncta. Depletion of microglia partially protects RGC function, despite loss of excitatory synapses, suggesting that activated microglia in the IPL are neurotoxic to RGC function early after transient IOP elevation. Taken together, the results of this study suggest that a driving factor for synapse disassembly after neuronal injury is the increased number of microglia at injury sites, which results in increased colocalization of microglia with synaptic components. Future work is needed to determine the role of microglia in active disassembly of intact synapses versus engulfment of synaptic material after ganglion cell death has already occurred, as well as the interplay between microglia and other cell types such as astrocytes.

As other groups have shown in mouse models of experimental glaucoma, microglia increase in density early and throughout the retina in response to IOP elevation.[14,16,32] These studies provided a large-scale examination of changes to microglia as a result of ocular hypertension in the different layers of the retina and at the optic nerve head. Our study focuses on the IPL and individual synapses to understand the role of microglia in the mechanism of synapse disassembly between RGCs and their presynaptic partners. Synapse loss as a result of increased IOP has been shown in multiple models of experimental glaucoma.[2,9,33,34] This phenomenon is also seen in other retinal diseases; in a model of retinitis pigmentosa, microglia are activated and increase phagocytosis of postsynaptic mGluR6,[35] a process thought to be complement-mediated. Aberrant synapse loss is also an early feature of other neurodegenerative diseases such as Alzheimer's disease, in which microglia play a key role in synapse loss.[36,37] After IOP elevation, we observed a significant increase in the number of pre- and postsynaptic puncta colocalized with microglia, driven by an increase in microglia density. The synaptic puncta colocalized inside microglia are significantly smaller in volume compared to synaptic puncta found outside of microglia, which suggests but does not definitively demonstrate that these synaptic components colocalized with microglia may have been phagocytosed or engulfed. In addition, the smaller size of engulfed puncta is consistent with microglia trogocytosis or "nibbling" of synapses, although we cannot rule out that microglia scavenge synaptic debris rather than engulfing intact synapses. However, analysis of individual ganglion cells shows that the synapses colocalized with microglia are located on structurally intact dendrites. Additionally, while the fraction of C1q within microglia is not increased in the laser vs. control condition, the individual ganglion cell results demonstrate that microglia target contact points where C1q is present on ganglion cell dendrites. Ultimately, live imaging of individual microglia and their interactions with C1q-tagged synaptic components is needed to define microglia function in disease conditions.

It is known that microglia in the CNS interact closely with neurons and play a role in maintenance of their function. This close contact to neurons and other glial cells allows microglia to respond quickly to stress. Here, we demonstrate that upon IOP elevation, the number of microglia contacting an individual RGC significantly increases resulting in a greater number of contact points as well as increased contact volume between microglia and RGCs. Thus, from the ganglion cell perspective, microgliosis results in greater contact at synaptic sites. However, even though microglia are likely in an activated state based on morphology, motility, and expression of CD68, this fixed tissue analysis does not definitively demonstrate that individual microglia increase their phagocytic activity. Indeed, as the density of synaptic components colocalized with each individual microglia does not increase after IOP elevation, this suggests that the increased synapse loss after injury is due to recruitment of additional microglia rather than simply microglia increasing their phagocytic capacity. Therefore, treatments that address the recruitment or infiltration of activated microglia, such as complement inhibition, may be an integral part of any therapeutic strategy targeting neuroinflammation.

Microglia responding to an injury signal has been shown in some contexts to be beneficial and neuroprotective; for example, clearance of stressed neurons by microglia in a glutamate-induced excitotoxicity model could help limit damage by phagocytosing hyperactive cells that are releasing neurodegenerative signals.[38] However, chronic activation of microglia is commonly associated with neurodegeneration and inhibition of microglial activation results in some neuroprotection. For example, investigators have treated animal models of glaucoma with minocycline, glucagon-like peptide-1 receptor (GLP-1R) agonists, such as NLY01 or commercially available GLP-1R agonists, and complement inhibitors in order to modulate microglia function and preserve RGC survival and/or synaptic integrity.[10,19,36,37] With evidence suggesting that microglia target excitatory postsynaptic sites after IOP elevation, we tested whether depleting microglia using PLX5622 for the duration of injury would preserve RGC function. Previous work by others depleting microglia using PLX5622 has resulted in variable outcomes: in an acute model of ocular hypertension[23] and the chronic DBA2/J mouse model,[24] microglia depletion using PLX5622 resulted in worse RGC loss, in an optic nerve crush model RGC loss was unaffected by microglia depletion,[21] and finally in an NMDA excitotoxicity model microglia depletion led to neuroprotection.[22] Here, we demonstrate that when microglia are depleted before laser-induced ocular hypertension and throughout the 7 days post-laser there is a significant preservation of RGC function as assessed by PERG. However, despite the preservation of function we did not observe preservation of synapse density along individual RGC dendrites, which may be due to several limitations. We only assessed alpha RGCs, whereas PERG assesses the function of all RGCs. In the absence of microglia, other glial cells such as astrocytes may be compensating for the lack of phagocytic activity from microglia.[39] Additionally, we know that microglia play a dynamic role in neuroprotection and neuroinflammation, so depleting them may have beneficial effects in one context and time point but may be detrimental in others. Indeed, we observed that PLX5622 treatment also decreased RGC synapse density in control eyes although no decrease in PERG function was observed. Indeed, microglia have been shown to be necessary for CNS synaptic maintenance in adulthood.[40] In the retina, Wang et al. found that microglia ablation resulted in a reduction in the b-wave of the ERG and degenerative changes in outer plexiform layer synapses on electron microscopy.[41] It is also possible that in the absence of microglia, remaining synaptic connections

increase their strength to compensate for decreased synapse density, resulting in partial preservation of PERG function. A comprehensive understanding of the timing, context, microglia-neuron crosstalk and interplay between microglia and other neuroinflammatory pathways including astrocytes, will benefit the development of novel therapeutics in diseases such as glaucoma where neuroinflammation is thought to play a significant role in its development and progression.

After transient IOP elevation, we previously demonstrated that RGC neurodegeneration is compartmentalized, with synapse loss preceding dendrite retraction and cell death and with synapse disassembly progressing in an IPL sublamina-dependent and ordered fashion with presynaptic component loss occurring prior to or simultaneously with postsynaptic component loss.[25] However, it was not known what role microglia play in synapse disassembly. Our findings here demonstrate that after transient IOP elevation, microglia increase in number, complexity, and motility, and this microgliosis is the driving factor for increased colocalization of microglia with synaptic components throughout the IPL and synaptic sites on ganglion cell dendrites. When microglia are depleted, we observe preservation of RGC function despite no corresponding rescue in synapse density. These findings underscore the complexity of microglia function in synapse disassembly during early stages of neurodegeneration. Identifying the precise mechanisms of microglia-synapse interactions and the relationship between microglia and injured neurons is critical to the design of novel therapeutics targeting neuroinflammation in neurodegenerative diseases such as glaucoma.

Limitations of the study

We acknowledge several limitations. First, our findings are limited to this specific experimental glaucoma model in mice, with use of the contralateral unlasered eye as control. Tribble et al. showed that microglial activation occurred in the contralateral (control) eye when ocular hypertension was induced unilaterally using magnetic microbead injection.[42] However, analyses performed in our laboratory demonstrated that naive eyes and contralateral eyes did not significantly differ in microglia density (data not shown). Furthermore, if microglia were appreciably activated in the contralateral eye, use of this eye as a control would not bias in favor of identifying differences between lasered vs. contralateral eye. Second, the majority of data analyzed originates from confocal microscopy examination of fixed tissue and therefore the analysis is hampered by the resolution limit of this technique. Nevertheless, the reported colocalization analysis method provides an objective measurement of fluorescent signal overlap and any limitation due to the resolution of the imaging modality equally affects control and lasered eyes. In addition, ongoing work using live imaging will reveal whether microglia are scavenging synaptic debris from apoptotic cells or engulfing intact synapses. Third, it is possible that some $CX_3CR\text{-}1^{GFP}$ cells are not resident or proliferating microglia but rather infiltrating monocyte-derived macrophages, for which a complete characterization would require lineage tracing. Fourth, microglia colocalization with excitatory postsynaptic sites may not be specific to ganglion cells, and indeed microgliosis likely impacts many elements of the circuit including other cell types. Finally, microglia were depleted with PLX5622 administered via chow, which may have off-target effects as its target, the CSF1 receptor, is expressed not only by microglia but also peripheral myeloid cells.[43] PLX5622 has also been shown to decrease astrocyte gap junction coupling.[44] Alternative tools to modulate microglia activity, such as via genetic manipulation of microglia function, would be useful for future studies.

RESOURCE AVAILABILITY

Lead contact

Further information and requests for resources and reagents should be directed to and will be fulfilled by Yvonne Ou (yvonne.ou@ucsf.edu).

Materials availability

The study did not generate new unique reagents.

Data and code availability

All data reported in this paper will be shared by the lead contact upon request. Data and code associated with the manuscript has been deposited in Zenodo: https://doi.org/10.5281/zenodo.14757201. All original code has been deposited at https://github.com/lucadellasantina and is publicly available as of the date of publication. DOIs are listed in the key resources table. Any additional information required to reanalyze the data reported in this paper is available from the lead contact upon request.

ACKNOWLEDGMENTS

The authors wish to thank Felice Dunn for helpful discussions and comments on the manuscript. We thank Yien-Ming Kuo for technical assistance and Suling Wang for assistance with graphics. This work is supported by NIH-NEI (EY028148 to Y.O.; EY300668 to A.L.; EY034973-01S1 to C.F.), E. Matilda Ziegler Foundation for the Blind (grant to Y.O.), BrightFocus Foundation (grants to Y.O. and A.L.), Nvidia Corporation (GPU grant to L.D.S.), Glaucoma Research Foundation (Shaffer grants to L.D.S. and Y.O.) and All May See Foundation (research grants to Y.O., L.D.S, L.X.T., and A.L.). This research was supported, in part, by the UCSF Vision Core shared resource of the NIH-NEI P30 EY002162, and by an unrestricted grant from Research to Prevent Blindness, New York, NY.

AUTHOR CONTRIBUTIONS

Conceptualization, Y.O. and L.D.S.; methodology, Y.O. and L.D.S., software, L.D.S., formal analysis, A.Y. and L.D.S.; investigation, A.Y., C.F., LXT., and Y.O., resources, A.L. and Y.O., writing—original draft, A.Y. and Y.O., writing—reviewing and editing, A.Y., L.D.S., L.X.T., A.L., and Y.O., supervision, Y.O., project administration, Y.O., funding acquisition, Y.O. and L.D.S.

DECLARATION OF INTERESTS

The authors declare no competing interests.

STAR★METHODS

Detailed methods are provided in the online version of this paper and include the following:

- KEY RESOURCES TABLE
- EXPERIMENTAL MODEL AND STUDY PARTICIPANT DETAILS
- METHOD DETAILS
  - Laser-induced ocular hypertension (LIOH)
  - Ballistic labeling of individual ganglion cells
  - Immunohistochemistry
  - EdU assay
  - Live imaging

- Microglia depletion
- Pattern electroretinogram (PERG)
- Image acquisition and analysis

- QUANTIFICATION AND STATISTICAL ANALYSIS

SUPPLEMENTAL INFORMATION

Supplemental information can be found online at https://doi.org/10.1016/j.isci.2025.112201.

Received: June 17, 2024
Revised: December 20, 2024
Accepted: March 6, 2025
Published: March 11, 2025

REFERENCES

1. Paolicelli, R.C., Bolasco, G., Pagani, F., Maggi, L., Scianni, M., Panzanelli, P., Giustetto, M., Ferreira, T.A., Guiducci, E., Dumas, L., et al. (2011). Synaptic Pruning by Microglia Is Necessary for Normal Brain Development. Science *333*, 1456–1458. https://doi.org/10.1126/science.1202529.
2. Stevens, B., Allen, N.J., Vazquez, L.E., Howell, G.R., Christopherson, K.S., Nouri, N., Micheva, K.D., Mehalow, A.K., Huberman, A.D., Stafford, B., et al. (2007). The Classical Complement Cascade Mediates CNS Synapse Elimination. Cell *131*, 1164–1178. https://doi.org/10.1016/j.cell.2007.10.036.
3. Schafer, D.P., Lehrman, E.K., Kautzman, A.G., Koyama, R., Mardinly, A.R., Yamasaki, R., Ransohoff, R.M., Greenberg, M.E., Barres, B.A., and Stevens, B. (2012). Microglia sculpt postnatal neural circuits in an activity and complement-dependent manner. Neuron *74*, 691–705. https://doi.org/10.1016/j.neuron.2012.03.026.
4. Li, Q., and Barres, B.A. (2018). Microglia and macrophages in brain homeostasis and disease. Nat. Rev. Immunol. *18*, 225–242. https://doi.org/10.1038/nri.2017.125.
5. Stevens, B., and Schafer, D.P. (2018). Roles of microglia in nervous system development, plasticity, and disease. Dev. Neurobiol. *78*, 559–560. https://doi.org/10.1002/dneu.22594.
6. Hong, S., and Stevens, B. (2016). Microglia: Phagocytosing to Clear, Sculpt, and Eliminate. Dev. Cell *38*, 126–128. https://doi.org/10.1016/j.devcel.2016.07.006.
7. Neufeld, A.H. (1999). Microglia in the Optic Nerve Head and the Region of Parapapillary Chorioretinal Atrophy in Glaucoma. Arch. Ophthalmol. *117*, 1050–1056. https://doi.org/10.1001/archopht.117.8.1050.
8. Bosco, A., Romero, C.O., Breen, K.T., Chagovetz, A.A., Steele, M.R., Ambati, B.K., and Vetter, M.L. (2015). Neurodegeneration severity can be predicted from early microglia alterations monitored in vivo in a mouse model of chronic glaucoma. Dis. Model. Mech. *8*, 443–455. https://doi.org/10.1242/dmm.018788.
9. Ou, Y., Jo, R.E., Ullian, E.M., Wong, R.O.L., and Della Santina, L. (2016). Selective Vulnerability of Specific Retinal Ganglion Cell Types and Synapses after Transient Ocular Hypertension. J. Neurosci. *36*, 9240–9252. https://doi.org/10.1523/JNEUROSCI.0940-16.2016.
10. Sterling, J.K., Adetunji, M.O., Guttha, S., Bargoud, A.R., Uyhazi, K.E., Ross, A.G., Dunaief, J.L., and Cui, Q.N. (2020). GLP-1 Receptor Agonist NLY01 Reduces Retinal Inflammation and Neuron Death Secondary to Ocular Hypertension. Cell Rep. *33*, 108271. https://doi.org/10.1016/j.celrep.2020.108271.
11. Della Santina, L., Yu, A.K., Harris, S.C., Soliño, M., Garcia Ruiz, T., Most, J., Kuo, Y.-M., Dunn, F.A., and Ou, Y. (2021). Disassembly and rewiring of a mature converging excitatory circuit following injury. Cell Rep. *36*, 109463. https://doi.org/10.1016/j.celrep.2021.109463.
12. Rutigliani, C., Tribble, J.R., Hagström, A., Lardner, E., Jóhannesson, G., Stålhammar, G., and Williams, P.A. (2022). Widespread retina and optic nerve neuroinflammation in enucleated eyes from glaucoma patients. acta neuropathol commun *10*, 1–13. https://doi.org/10.1186/s40478-022-01427-3.
13. Margeta, M.A., Yin, Z., Madore, C., Pitts, K.M., Letcher, S.M., Tang, J., Jiang, S., Gauthier, C.D., Silveira, S.R., Schroeder, C.M., et al. (2022). Apolipoprotein E4 impairs the response of neurodegenerative retinal microglia and prevents neuronal loss in glaucoma. Immunity *55*, 1627–1644.e7. https://doi.org/10.1016/j.immuni.2022.07.014.
14. Bosco, A., Steele, M.R., and Vetter, M.L. (2011). Early microglia activation in a mouse model of chronic glaucoma. J. Comp. Neurol. *519*, 599–620. https://doi.org/10.1002/cne.22516.
15. Krishnan, A., Kocab, A.J., Zacks, D.N., Marshak-Rothstein, A., and Gregory-Ksander, M. (2019). A small peptide antagonist of the Fas receptor inhibits neuroinflammation and prevents axon degeneration and retinal ganglion cell death in an inducible mouse model of glaucoma. J. Neuroinflammation *16*, 184. https://doi.org/10.1186/s12974-019-1576-3.
16. Ramírez, A.I., Fernández-Albarral, J.A., Hoz, R.d., López-Cuenca, I., Salobrar-García, E., Rojas, P., Valiente-Soriano, F.J., Avilés-Trigueros, M., Villegas-Pérez, M.P., Vidal-Sanz, M., et al. (2020). Microglial changes in the early aging stage in a healthy retina and an experimental glaucoma model. Prog. Brain Res. *256*, 125–149. https://doi.org/10.1016/bs.pbr.2020.05.024.
17. Tribble, J.R., Harder, J.M., Williams, P.A., and John, S.W.M. (2020). Ocular hypertension suppresses homeostatic gene expression in optic nerve head microglia of DBA/2 J mice. Mol. Brain *13*, 81. https://doi.org/10.1186/s13041-020-00603-7.
18. Baptiste, D.C., Powell, K.J., Jollimore, C.A.B., Hamilton, C., Levatte, T.L., Archibald, M.L., Chauhan, B.C., Robertson, G.S., and Kelly, M.E.M. (2005). Effects of minocycline and tetracycline on retinal ganglion cell survival after axotomy. Neuroscience *134*, 575–582. https://doi.org/10.1016/j.neuroscience.2005.04.011.
19. Bosco, A., Inman, D.M., Steele, M.R., Wu, G., Soto, I., Marsh-Armstrong, N., Hubbard, W.C., Calkins, D.J., Horner, P.J., and Vetter, M.L. (2008). Reduced Retina Microglial Activation and Improved Optic Nerve Integrity with Minocycline Treatment in the DBA/2J Mouse Model of Glaucoma. Investig. Ophthalmol. Vis. Sci. *49*, 1437–1446. https://doi.org/10.1167/iovs.07-1337.
20. Bosco, A., Crish, S.D., Steele, M.R., Romero, C.O., Inman, D.M., Horner, P.J., Calkins, D.J., and Vetter, M.L. (2012). Early Reduction of Microglia Activation by Irradiation in a Model of Chronic Glaucoma. PLoS One *7*, e43602. https://doi.org/10.1371/journal.pone.0043602.
21. Hilla, A.M., Diekmann, H., and Fischer, D. (2017). Microglia Are Irrelevant for Neuronal Degeneration and Axon Regeneration after Acute Injury. J. Neurosci. *37*, 6113–6124. https://doi.org/10.1523/JNEUROSCI.0584-17.2017.
22. Takeda, A., Shinozaki, Y., Kashiwagi, K., Ohno, N., Eto, K., Wake, H., Nabekura, J., and Koizumi, S. (2018). Microglia mediate non-cell-autonomous cell death of retinal ganglion cells. Glia *66*, 2366–2384. https://doi.org/10.1002/glia.23475.
23. Tan, Z., Guo, Y., Shrestha, M., Sun, D., Gregory-Ksander, M., and Jakobs, T.C. (2022). Microglia depletion exacerbates retinal ganglion cell loss in a mouse model of glaucoma. Exp. Eye Res. *225*, 109273. https://doi.org/10.1016/j.exer.2022.109273.
24. Diemler, C.A., MacLean, M., Heuer, S.E., Hewes, A.A., Marola, O.J., Libby, R.T., and Howell, G.R. (2024). Microglia Depletion leads to Increased Susceptibility to Ocular Hypertension-Dependent Glaucoma. Front. Aging Neurosci. *16*, 1396443. https://doi.org/10.3389/fnagi.2024.1396443.
25. Soliño, M., Yu, A., Della Santina, L., and Ou, Y. (2023). Large-Scale Survey of Excitatory Synapses Reveals Sublamina-Specific and Asymmetric Synapse Disassembly Patterns in a Neurodegenerative Circuit. iScience *26*, 107262. https://doi.org/10.1016/j.isci.2023.107262.
26. Fu, C.T., and Sretavan, D. (2010). Laser-induced ocular hypertension in albino CD-1 mice. Investig. Ophthalmol. Vis. Sci. *51*, 980–990. https://doi.org/10.1167/iovs.09-4324.

27. Li, S., Woodfin, M., Long, S.S., and Fuerst, P.G. (2016). IPLaminator: an ImageJ plugin for automated binning and quantification of retinal lamination. BMC Bioinf. *17*, 36. https://doi.org/10.1186/s12859-016-0876-1.

28. Object Finder : 3D object recognition in image volumes https://lucadellasantina.github.io/ObjectFinder/.

29. Weinhard, L., di Bartolomei, G., Bolasco, G., Machado, P., Schieber, N.L., Neniskyte, U., Exiga, M., Vadisiute, A., Raggioli, A., Schertel, A., et al. (2018). Microglia remodel synapses by presynaptic trogocytosis and spine head filopodia induction. Nat. Commun. *9*, 1228. https://doi.org/10.1038/s41467-018-03566-5.

30. Krieger, B., Qiao, M., Rousso, D.L., Sanes, J.R., and Meister, M. (2017). Four alpha ganglion cell types in mouse retina: Function, structure, and molecular signatures. PLoS One *12*, e0180091. https://doi.org/10.1371/journal.pone.0180091.

31. Porciatti, V. (2015). Electrophysiological assessment of retinal ganglion cell function. Exp. Eye Res. *141*, 164–170. https://doi.org/10.1016/j.exer.2015.05.008.

32. de Hoz, R., Ramírez, A.I., González-Martín, R., Ajoy, D., Rojas, B., Salobrar-Garcia, E., Valiente-Soriano, F.J., Avilés-Trigueros, M., Villegas-Pérez, M.P., Vidal-Sanz, M., et al. (2018). Bilateral early activation of retinal microglial cells in a mouse model of unilateral laser-induced experimental ocular hypertension. Exp. Eye Res. *171*, 12–29. https://doi.org/10.1016/j.exer.2018.03.006.

33. Della Santina, L., Inman, D.M., Lupien, C.B., Horner, P.J., and Wong, R.O.L. (2013). Differential progression of structural and functional alterations in distinct retinal ganglion cell types in a mouse model of glaucoma. J. Neurosci. *33*, 17444–17457. https://doi.org/10.1523/JNEUROSCI.5461-12.2013.

34. Berry, R.H., Qu, J., John, S.W.M., Howell, G.R., and Jakobs, T.C. (2015). Synapse Loss and Dendrite Remodeling in a Mouse Model of Glaucoma. PLoS One *10*, e0144341. https://doi.org/10.1371/journal.pone.0144341.

35. He, J., Zhao, C., Dai, J., Weng, C.H., Bian, B.S.J., Gong, Y., Ge, L., Fang, Y., Liu, H., Xu, H., and Yin, Z.Q. (2019). Microglia Mediate Synaptic Material Clearance at the Early Stage of Rats With Retinitis Pigmentosa. Front. Immunol. *10*, 912. https://doi.org/10.3389/fimmu.2019.00912.

36. Henstridge, C.M., Hyman, B.T., and Spires-Jones, T.L. (2019). Beyond the neuron–cellular interactions early in Alzheimer disease pathogenesis. Nat. Rev. Neurosci. *20*, 94–108. https://doi.org/10.1038/s41583-018-0113-1.

37. Hong, S., Beja-Glasser, V.F., Nfonoyim, B.M., Frouin, A., Li, S., Ramakrishnan, S., Merry, K.M., Shi, Q., Rosenthal, A., Barres, B.A., et al. (2016). Complement and microglia mediate early synapse loss in Alzheimer mouse models. Science *352*, 712–716. https://doi.org/10.1126/science.aad8373.

38. Noda, M., Doi, Y., Liang, J., Kawanokuchi, J., Sonobe, Y., Takeuchi, H., Mizuno, T., and Suzumura, A. (2011). Fractalkine attenuates excito-neurotoxicity via microglial clearance of damaged neurons and antioxidant enzyme heme oxygenase-1 expression. J. Biol. Chem. *286*, 2308–2319. https://doi.org/10.1074/jbc.M110.169839.

39. Konishi, H., Okamoto, T., Hara, Y., Komine, O., Tamada, H., Maeda, M., Osako, F., Kobayashi, M., Nishiyama, A., Kataoka, Y., et al. (2020). Astrocytic phagocytosis is a compensatory mechanism for microglial dysfunction. EMBO J. *39*, e104464. https://doi.org/10.15252/embj.2020104464.

40. Basilico, B., Ferrucci, L., Ratano, P., Golia, M.T., Grimaldi, A., Rosito, M., Ferretti, V., Reverte, I., Sanchini, C., Marrone, M.C., et al. (2022). Microglia control glutamatergic synapses in the adult mouse hippocampus. Glia *70*, 173–195. https://doi.org/10.1002/glia.24101.

41. Wang, X., Zhao, L., Zhang, J., Fariss, R.N., Ma, W., Kretschmer, F., Wang, M., Qian, H.H., Badea, T.C., Diamond, J.S., et al. (2016). Requirement for Microglia for the Maintenance of Synaptic Function and Integrity in the Mature Retina. J. Neurosci. *36*, 2827–2842. https://doi.org/10.1523/JNEUROSCI.3575-15.2016.

42. Tribble, J.R., Kokkali, E., Otmani, A., Plastino, F., Lardner, E., Vohra, R., Kolko, M., André, H., Morgan, J.E., and Williams, P.A. (2021). When Is a Control Not a Control? Reactive Microglia Occur Throughout the Control Contralateral Pathway of Retinal Ganglion Cell Projections in Experimental Glaucoma. Transl. Vis. Sci. Technol. *10*, 22. https://doi.org/10.1167/tvst.10.1.22.

43. Green, K.N., Crapser, J.D., and Hohsfield, L.A. (2020). To Kill a Microglia: A Case for CSF1R Inhibitors. Trends Immunol. *41*, 771–784. https://doi.org/10.1016/j.it.2020.07.001.

44. Du, Y., Brennan, F.H., Popovich, P.G., and Zhou, M. (2022). Microglia maintain the normal structure and function of the hippocampal astrocyte network. Glia *70*, 1359–1379. https://doi.org/10.1002/glia.24179.

STAR★METHODS

KEY RESOURCES TABLE

REAGENT or RESOURCE	SOURCE	IDENTIFIER
Antibodies		
anti-CtBP2 mouse IgG1 monoclonal antibody	BD Biosciences	Cat # 612044 RRID:AB_399431
anti-PSD95 mouse IgG2a monoclonal antibody	Neuromab	Cat# 73-028; RRID:AB_10698024
anti-CD68 rat monoclonal antibody	Bio-Rad	Cat# MCA1957; RRID: AB_322219
anti-C1q rabbit monoclonal antibody	Abcam	Cat# ab182451; RRID: AB_2732849
DyLight 405 AffiniPure Goat Anti-Mouse IgG, Fcg subclass 1 specific	Jackson ImmunoResearch	Cat # 115-475-205; RRID:AB_2338799
DyLight™ 405 AffiniPure Goat Anti-Rat IgG (H + L)	Jackson ImmunoResearch	Cat# 112-475-003; RRID: AB_2338303
Alexa Fluor® 647 AffiniPure Goat Anti-Mouse IgG, Fcγ subclass 2a specific	Jackson ImmunoResearch	Cat# 115-605-206; RRID: AB_2338917
Critical commercial assays		
Click-iT™ Plus EdU Cell Proliferation Kit for Imaging, Alexa Fluor™ 555 dye	Invitrogen	Cat# C10337
Chemicals, peptides, and recombinant proteins		
Dextran, Alexa Fluor™ 568; 10,000 MW, Anionic, Fixable	Invitrogen	Cat# D22912
PLX5622	Chemgood	Cat# C-1521
Experimental models: organisms/strains		
B6.129P2(Cg)-Cx3cr1tm1Litt/J	The Jackson Laboratory	Strain #:005582; RRID:IMSR_JAX:005582
CD-1 albino mice (Crl:CD1(ICR) Outbred)	Charles River Laboratories	RRID:IMSR_CRL:022
Software and algorithms		
Imaris	Bitplane	RRID:SCR_007370
VolumeCut	https://github.com/lucadellasantina/VolumeCut	https://doi.org/10.5281/zenodo.5048331
ImageJ	NIH	RRID:SCR_003070
ObjectFinder	https://github.com/lucadellasantina/ObjectFinder	https://doi.org/10.5281/zenodo.4767847
Mann-Whitney U Calculator	Social Science Statistics	https://www.socscistatistics.com/tests/mannwhitney/default.aspx
MATLAB	MathWorks	RRID:SCR_001622
Deposited data		
Zenodo	OpenAIRE	https://doi.org/10.5281/zenodo.14757201

EXPERIMENTAL MODEL AND STUDY PARTICIPANT DETAILS

Male and female CD-1 albino mice (Charles River; strain 022) were crossed with B6.129P2(Cg)-*Cx3cr1*^{tm1Litt}/J (The Jackson Laboratory; strain 005582) to produce CD-1 albino mice with EGFP-expressing microglia. Experimental animals included male and female Cx3cr1 heterozygous mice produced after a minimum of 4 generations of backcrossing. This strain was maintained and refreshed after 10 generations back onto the CD-1 background to prevent genetic drift. Littermates of the same sex were assigned to experimental groups. Animals were housed in animal facilities at the University of California, San Francisco. Mice were exposed to daily light cycles of 12 h light and 12 h dark, and given water and standard diet *ad libitum* except when specified. All procedures were performed as approved by the Institutional Animal care and Use Committees at the University of California, San Francisco under protocol number AN203526.

METHOD DETAILS

Laser-induced ocular hypertension (LIOH)

Female and male mice 2–3 months of age were anesthetized with intraperitoneal injection of ketamine (100 mg/kg) and xylazine (10 mg/kg). Baseline IOP measurement was taken with the Tonolab rebound tonometer (Colonial Medical Co. Inc.). Each measurement was triggered with a custom foot pedal to minimize movement of the device. A total of 3 measurements per eye (each measurement is an average of 6 readings) were taken. Ocular hypertension was induced in the left eye with an endoprobe attached to a diode laser (532 nm; Lumenis) that photocoagulated the limbal and at least 3–6 episcleral vessels in the left eye (300 mW laser power, 0.5 s duration, 100 μm diameter spot size, about 80–100 total spots. The translimbal laser treatment covered 330° sparing the nasal aspect and the long posterior ciliary arteries. Lubricant ophthalmic ointment was then applied to the lasered eye and the non-lasered right eye served as the control. IOP measurements were taken daily for 7 days post-laser under isoflurane at approximately the same time of day. Gross examination of the eyes during IOP measurements were noted and eyes that exhibited corneal edema, hyphema, inflammation, and IOP >50 mmHg were excluded from the study.

Ballistic labeling of individual ganglion cells

Seven days after LIOH mice were anesthetized with isoflurane and euthanized by cervical dislocation. Eyes were carefully removed and placed in oxygenated ACSF (pH 7.4) with the following components in mm: 119 NaCl, 2.5 KCl, 1.3 $MgCl_2 \cdot 6H_2O$, 2.5 $CaCl_2 \cdot 2H_2O$, 1 $NaHPO_4$, 11 glucose, and 20 HEPES. Retinas were then dissected from the eyecup and mounted onto nitrocellulose filter paper (Millipore). Dextran-568 coated tungsten particles were prepared (Morgan & Wong, 2008) and a helium-pressured (40 psi) Helios gene gun (Bio-Rad) was used to ballistically deliver the tungsten particles onto the retinas. Within 5 min confirmation of cell fill was visualized on a fluorescent cell imager (Bio-Rad). The retinas were then quickly fixed with 2% paraformaldehyde for 30 min and washed twice with 1x PBS.

Immunohistochemistry

Fixed retinas were incubated in blocking solution (5% normal donkey serum (Jackson ImmunoResearch), 2% BSA (Sigma), and 0.05% Triton X-100 (Sigma) in 1x PBS) overnight at 4°C. Primary antibodies are then diluted in blocking solution and incubated for 4 nights at 4°C. The retinas were incubated with the following primary antibodies: anti-CtBP2 (mouse IgG1 1:500; BD Biosciences); anti-PSD95 (mouse IgG2a 1:500; Neuromab); rabbit monoclonal anti-C1q (1:500; Abcam); rat monoclonal anti-CD68 (1:500; Bio-Rad). After washing with 0.03% Triton X-100 in PBS, the appropriate secondary antibodies were incubated overnight at 4°C (Alexa , Invitrogen, 1:1000; or Dylight, Jackson ImmunoResearch, 1:1000, conjugated fluorophores). After washing again, the retinas were mounted with Vectashield (Vector Laboratories) onto glass slides.

EdU assay

Click-iT Plus EdU Proliferation Kit (Invitrogen) was used to determine cells that are undergoing proliferation during the 7 days post-LIOH. EdU was dosed (50 mg/mg) every day starting at day 0 to day 6 with a 5 mg/mL stock solution. After euthanasia at 7 days post-LIOH retinas were dissected and flatmounted to detect EdU+ cells.

Live imaging

Imaging was performed at room temperature in an Okolab humidified microenvironmental chamber on a Nikon spinning disk confocal microscope with a 60× objective (NA 1.49). The system is equipped with: Yokogawa CSU-X1 confocal spinning disk head, Nikon Eclipse Ti2-E inverted microscope, Live-SR super-resolution module, Andor iXon Ultra 888 EMCCD camera, TI2-S-SE-E motorized stage with piezo-Z for rapid z stack acquisition, and a laser combiner with four solid-state lasers at 405, 488, 561, and 640 nm and the corresponding band-pass emission filter sets (Chroma) loaded on an FLI high speed filter wheel. Time-lapse image stacks of microglia in the IPL were acquired every 20 s for a total of 5–10 min. Retinas were flattened and mounted on nitrocellulose filter paper and placed ganglion cell side face down onto a glass bottom Petri dish. The Petri dish is filled with oxygenated ACSF and the retina and filter paper is weighed down with a stainless steel wire to prevent drifting, with freshly oxygenated ACSF replenished after each acquisition.

Two to six microglia were analyzed per retina. All processes of all fully intact microglia within the image stack were analyzed. To quantify microglia process displacement and speed, surface rendering was performed in Imaris 10.2, using the ''AI Machine Learning Segmentation'' algorithm that was iteratively adjusted via manual training and verification that each mask was accurate. The entire microglia was masked and its cell movement was tracked in each z stack at 20s intervals. Detected process movement was confirmed by manually scrolling through each time lapse. Surface displacement length and speed statistics were extracted and recorded as average process displacement and average process speed, respectively.

Microglia depletion

PLX5622 (Chemgood), a CSF-1R inhibitor, was mixed in standard AIN-76A rodent diet at 1200 ppm (Research Diets) and given to the mice *ad libitum*. PLX5622 was administered to the mice 2 weeks prior to LIOH and they remained on the PLX5622 diet until euthanasia at 7 days post-LIOH.

Pattern electroretinogram (PERG)

Inner retinal function will be assessed using noninvasive corneal PERG recording. The PERG signal is generated by presentation of a contrast reversing grating pattern, which results in a nonlinear signal that is dependent on the functional integrity of the retinal ganglion cells (RGCs) (Porciatti, 2007). Mice were anesthetized with ketamine (100 mg/kg) and xylazine (10 mg/kg) and pupils were dilated with a drop of 1% tropicamide. Genteal (Alcon) lubricating gel was used to keep the eyes from drying and used as a coupling agent during the recording. Using the Celeris ERG system (Diagnosys), a sinusoidal grating was presented to the mouse with a background light intensity of 50 cd s/m^2 at 100% contrast and 0.155 cycles per degree. A corneal electrode is placed on the other eye as a reference. The unit is heated to 37°C to keep the mouse warm. Two sets of 300 sweeps are presented to the mouse and averaged. Once completed the PERG stimulator was placed on the other eye and the recording procedure was repeated. Positive P1 amplitude is then quantified from the N1 trough to the P1 peak; and Negative N2 amplitude is measured from the P1 peak to the N2 trough.

Image acquisition and analysis

Confocal image stacks were acquired with pixel dimensions of 0.098 × 0.098 × 0.3 μm using an upright microscope (Leica SP8) with a 63× oil immersion objective (NA 1.40). For whole IPL analysis of microglia image stacks were acquired in the central retina at the 4 leaflets of the whole mounted retina. For single cell analysis, individual alpha ganglion cells were identified and the whole IPL was imaged to determine if the dendrites stratified in the OFF or ON sublamina. To remove thermal noise from the microscope detectors, image stacks were median filtered (kernel size 1 × 1 × 1 voxels) and converted to 8-bit.

Individual alpha RGCs and all microglia were skeletonized using the filament function in Imaris (Bitplane) and binary masks were produced by fitting to their prospective signal. The IPL was then segmented from the image stack using VolumeCut by identifying the IPL margins with the CtBP2 immunofluorescent labeling, which dimly labels nuclei of neurons in the adjacent nuclear layers (INL and GCL). PSD95 and CtBP2 puncta were then identified using ObjectFinder and colocalization analysis with ObjectFinder identified puncta that are correlated with microglia or the individual alpha RGC. To assess which synaptic puncta was colocalized to microglia and individual RGC, we required that 100% of the puncta signal was contained within the microglia or RGC binary mask. The image acquisition and analysis pipeline is visually summarized in Figure S1A.

QUANTIFICATION AND STATISTICAL ANALYSIS

Unless otherwise specified, all data reported represent mean ± SEM. Statistical significance was analyzed using the Mann-Whitney U test with significance defined as $p < 0.05$ (Mann-Whitney *U* Test calculator (2022, February 15); retrieved from https://www.socscistatistics.com/tests/mannwhitney/default.aspx). The number of cells/animals are reported in each histogram as well as in the figure legend.

Statistical comparison for PLX5622 experiments was performed using an ANOVA model with interaction between the two factors, diet (regular versus PLX5622) and treatment (control versus LIOH), followed by multiple comparisons using Tukey-Kramer test using MATLAB (MathWorks). All statistical tests and *p* values are included in a Table S1.